

# Sorption Phenomena In Transient Vapor Intrusion Scenarios

Jonathan G. V. Ström<sup>a</sup>, Shuai Xie<sup>a</sup>, Eric M. Suuberg<sup>a</sup>

*These authors contributed equally to this work*

<sup>a</sup>*Brown University, School of Engineering, Providence, RI, USA*

---

## Abstract

Many vapor intrusion (VI) contaminants have the capacity to sorb onto a variety of materials commonly found in buildings as well as soils, yet the role and effect of sorption in VI is largely unstudied. To bridge this gap we measure the sorptive capacities of trichloroethylene (TCE) on some materials at VI relevant concentrations; finding that material sorptive capacities vary orders of magnitudes, with cinderblock having a capacity to hold up to almost 41,000 times more contaminant than a comparable TCE contaminated air volume. Using these experimentally derived data together with a three-dimensional numerical model of VI, we then explore the retarding effect that sorption has on contaminant transport in soils and indoor environments. We also apply the model to investigate how the contaminant desorption from these materials, following the implementation of a successful VI mitigation scheme, affect contaminant expulsion. We find that desorption may cause significant delay: in some cases taking months longer than if there were no sorbed contaminants.

*Keywords:* Vapor intrusion, Temporal variability, Sorption, Attenuation factor, Mitigation

---

## 1. Introduction

Most vapor intrusion (VI) contaminants have the capacity to sorb onto soil and various common indoor materials, but the role and more importantly, the consequences of these sorption processes in VI are poorly understood[1, 2, 3]. The migration of contaminant vapors from their source into the VI impacted building and potential indoor sources is usually the prime concern

15 in VI investigations. Rarely are the sorbed contaminant vapors in the soil or  
16 indoor considered in an investigation. These may potentially act as a capac-  
17 itance, storing and releasing contaminant vapors in response to a change in  
18 contaminant concentration. Consequently, contaminant vapors may be more  
19 persistent than expected at a site that has undergone remediation, poten-  
20 tially reducing the effectiveness of mitigation in the short term, or leading to  
21 misleading results regarding mitigation efficacy.

22 It is well recognized that building materials have the capacity to sorb pol-  
23 lutants. The sorptive capacity of various volatile organic compounds (VOCs)  
24 of concern in VI has been examined on a variety of building materials, such as  
25 particle density board[4], gypsum wallboard[5], and plywood and carpets[6].  
26 However, most of these studies used relative high contaminant concentra-  
27 tions, usually around  $\text{mg}/\text{m}^3$ [4] or even higher. This is several orders of  
28 magnitude higher than the concentrations relevant in VI and due to the non-  
29 linear nature of sorption with respect to concentration, sorption studies at  
30 lower concentration are needed.

31 Many VOC sorption studies have also focused on the interaction between  
32 building materials and formaldehyde[5], toluene, and decane[6]. However,  
33 one of the contaminants of greatest concern in VI - trichloroethylene (TCE),  
34 has not received attention. This is despite the fact that sorption of TCE  
35 (and other comparable VOCs) on activated carbon is extensively used to  
36 treat indoor air contamination and their sorption on passive tube samplers  
37 is widely employed for analysis of these compounds[7].

38 Over the years many VI sites have been investigated. Two well-known  
39 examples of these are the studies of a house in Layton, Utah and one in In-  
40 dianapolis, Indiana. Both of these sites were outfitted with a wide variety of  
41 instrumentation to measure various metrics such as contaminant concentra-  
42 tion in interior, soil, and groundwater, as well as pressure, temperature, or  
43 weather. These studies yielded some of the richest VI datasets available and  
44 gave invaluable insights into the VI process, including into the application  
45 of CPM[8] and sub-slab depressurization (SSD) mitigation systems[9, 10].  
46 However, neither of these studies considered the role that sorption may have  
47 had at these sites.

48 The potential impact of sorption could perhaps be most significant in situ-  
49 ations in which contaminant entry rates vary widely with time, such as in the  
50 application of the controlled pressure method (CPM) and various mitigation  
51 schemes. The controlled pressure method involves the forced over- and de-  
52 pressurization of a building to maximize or minimize the contaminant entry

rate into the building. This can help the investigator ascertain the worst-case VI scenario and help identify potential indoor contaminant sources[11, 8]. However, if the building indoor materials have a large sorptive capacities, then desorption and sorption processes may significantly affect the indoor air contaminant concentration. Likewise, a significant amount of sorbed contaminant may be released from interior materials over an unknown period of time after mitigating the contaminant intrusion at a site[1, 2].

In the past, VI models have been used to gain further insight into VI processes[12, 13, 14]. Previous examples of VI modeling studies include one on the role of rainfall in VI[15], or drivers of temporal variability in some of the aforementioned sites[16]. However, while many VI models are presented including a sorption term in the governing equation for contaminant transport in soils, none have really explored the role of sorption in VI in a transient simulation. The reason for this is two-fold. First, there has been a general lack of interest in sorption related to VI thus far. Secondly, the vast majority of VI modeling efforts and studies have focused on steady-state analyses of VI, and sorption only affects soil contaminant transport in time-dependent scenarios.

To bridge this knowledge gap we will explore the role of sorption in VI by considering the significance of newly obtained contaminant sorption data in the context of VI models. Sorption data of TCE on various materials, including cinderblock, drywall, wood, paper, carpet, and Applying soil have been measured in a fixed bed sorption experiment. These sorption data are used to generate sorption parameters to be used in a three-dimensional finite element VI model. For this purpose we will consider a prototypical VI scenario where a free-standing house, with a basement, is overlying a homogeneously contaminated groundwater source. Using this model we investigate how contaminant transport is affected by sorption, how indoor sorptive materials affect indoor air concentration as the building’s pressurization fluctuates and how indoor air concentration are affected by indoor materials following successful mitigation of the structure.

## 2. Methods

### 2.1. Experimental Setup

The details of the experiments used in obtaining the sorption input data will be discussed in a separate paper being prepared on this topic. Here, we only briefly summarize the experiments.

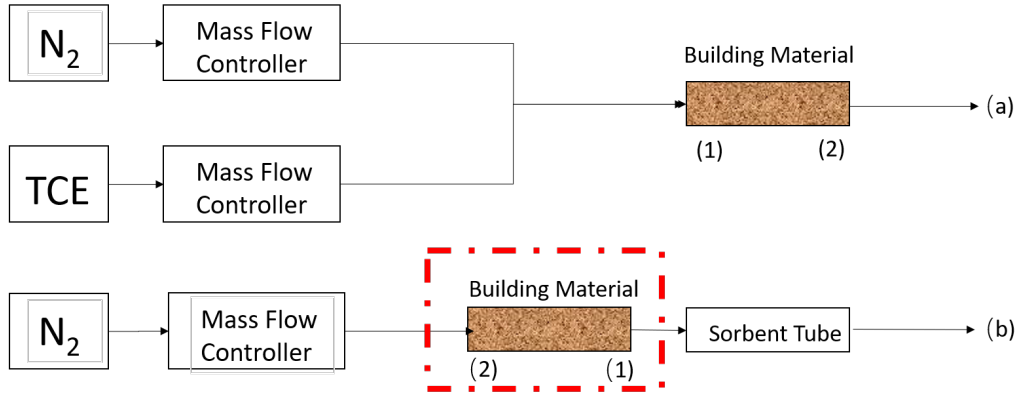


Figure 1: Schematic of experimental setup.

To study the dynamic sorption of TCE onto the selected building materials, the two-step process shown in Figure 1 was used.

A 7.5 by 1.27 cm stainless steel column was filled with a ground sample of the material to be tested. We use 2.0 g of drywall, and 1.0 g of all the other materials to pack the tube. Samples were held in by glass wool plugs. Using flow controllers, TCE was diluted in nitrogen gas to 1.12 ppb<sub>v</sub> and flowed through the column at a rate of 60 mL per minute, for a pre-selected time period. After the material had been exposed for the selected time, the column was detached and attached to the desorption system.

In the desorption system, the sample-containing column was heated to 100 °C and pure nitrogen gas was flowed through the previously outlet side of the column - carrying the desorbed contaminant with it. The gas was then passed through a long tube, allowing the gas to cool to room temperature, from which it flowed into a carbon-filled stainless steel sorption column which trapped all of the TCE for analysis. The sorption column was then desorbed into a gas-chromatograph fitted with a electron capture detector.

## 2.2. Numerical Model

To investigate the role of sorption in VI, we developed a three-dimensional numerical model of a building overlying a TCE contaminated groundwater source in the commercial finite-element solver COMSOL. The building is assumed to have a 10 by 10 m footprint, with a 3 meter ceiling height, and its foundation is located 1 m below ground surface (bgs). The contaminated groundwater is 4 m bgs, and is assumed to be homogenously contaminated with TCE. The building is surrounded by homogenous soil, that extends 10

113 m from its walls. Along the perimeter of the foundation, there is a 1 cm wide  
114 crack through which contaminant vapors enter the building and expulsion of  
115 contaminant vapors from the indoor occurs through air exchange with the  
116 outside.

117 Contaminant vapors are transported from the contaminated groundwater  
118 through the soil matrix via advection and diffusion and is described in 2.2.3.  
119 The presence of the groundwater variably saturates the soil matrix with  
120 water, which has a significant effects on the contaminant transport and is  
121 modeled using van Genuchten’s retention model[17] and explained in greater  
122 detail in section 2.2.1. The water in the soil matrix is assumed to be sta-  
123 tionary, thus advective transport only occurs through the vapor phase, while  
124 diffusion occurs through both the water and the vapor phases. The contam-  
125 inant vapors are also assumed to be able to sorb onto the soil particles, and  
126 is modeled using a linear sorption model, and the interaction between the  
127 water and vapor phases are determined by Henry’s Law.

128 The building is assumed to be pressurized relative to the outside, which  
129 gives an air flow in and out of the building (depending on if it is depressurized  
130 or overpressurized). This air flow causes the advective contaminant transport  
131 through the soil and the foundation crack. Darcy’s Law is used to model the  
132 flow of air and is described in detail in section 2.2.2. A key assumption here  
133 is that the contaminant is so diluted in the air, that it is assumed to not  
134 affect the transport properties of air.

135 In our implementation, only the soil surrounding the building is explicitly  
136 modeled (as a three-dimensional geometry), and the interior of the basement  
137 is implicitly modeled as a continuously stirred tank reactor as described in  
138 section 2.2.4. These two are coupled via the foundation crack, from which  
139 the contaminant entry into the basement is calculated, and contaminant  
140 expulsion is determined by the air exchange rate. In this work we consider  
141 the role of sorption on materials in the interior, which is done as a equilibrium  
142 reaction.

143 An overview of this modeling approach may be seen in Figure 2.

#### 144 2.2.1. Vadose Zone Moisture Content

145 Since the contaminant transport occurs through the three-phase vadose  
146 zone, it is important that we correctly account for soil moisture content and  
147 its effect on advective and diffusive transport. In this modeled scenario, we  
148 assume that the soil moisture is at steady-state, and thus the soil moisture  
149 content is given by the retention model developed by van Genuchten[17].

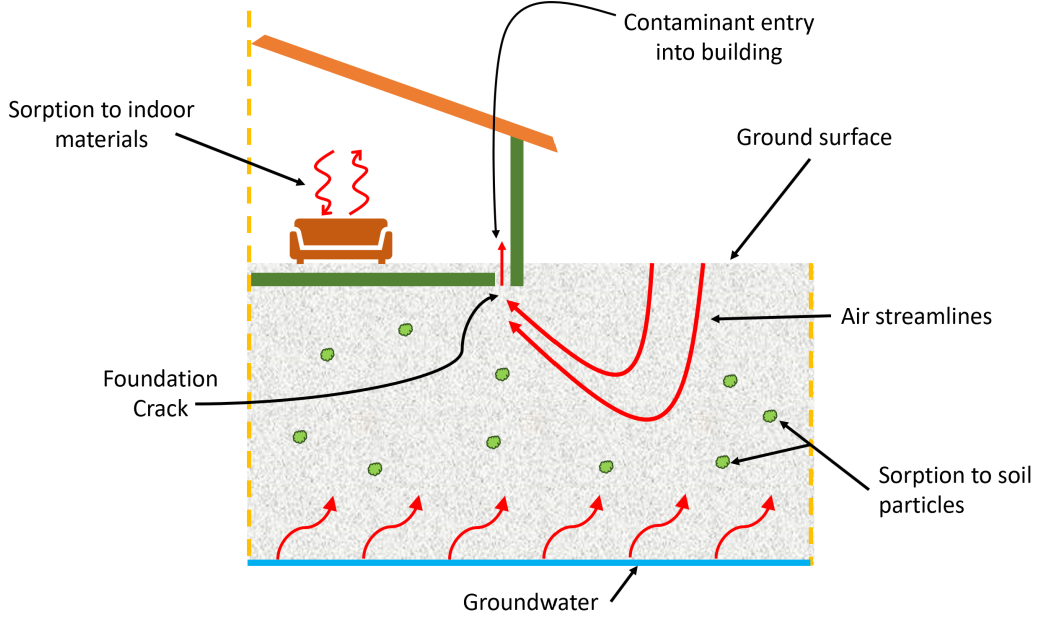


Figure 2: A schematic of the modeled vapor intrusion scenario.

The van Genuchten retention model gives the soil water saturation as a function of elevation above groundwater. This in turn gives the water and gas filled porosities in the soil, and the relative permeability of the soil matrix.

$$Se = \begin{cases} \frac{1}{(1+\alpha z^n)^m} & z < 0 \\ 1 & z \geq 0 \end{cases} \quad (1)$$

$$\theta_w = \begin{cases} \theta_r + Se(\theta_s - \theta_r) & z < 0 \\ \theta_s & z \geq 0 \end{cases} \quad (2)$$

$$k_r = \begin{cases} Se^l [1 - (1 - Se^{\frac{1}{m}})]^2 & z < 0 \\ 0 & z \geq 0 \end{cases} \quad (3)$$

150 Se is the saturation, and ranges from 0 to 1, which represent completely  
 151 unsaturated to fully saturated;  $z$  is a height relative to groundwater in meters,  
 152 with  $z = 0$  the groundwater surface and  $z < 0$  into the vadose zone;  $\theta_r$ ,  $\theta_s$ ,  
 153  $\theta_w$ , and  $\theta_g$  are the dimensionless porosity parameters reflecting the residual  
 154 moisture content, saturated porosity (or just porosity), and water and air  
 155 filled porosities respectively;  $k_r$  is the relative permeability of water transport  
 156 and  $1 - k_r$  gives the relative permeability of air transport.

157 *2.2.2. Gas Flow In The Vadose Zone*

158 The gas flow in the vadose zone is governed by a modified version of  
 159 Darcy's Law. Originally, Darcy's Law was developed to describe flow in satu-  
 160 rated porous media; but flow in unsaturated media requires some modification[18].  
 161 An effective permeability that depends on the relative permeability given by  
 162 the van Genuchten equations is introduced to allow for correct permeability  
 163 in unsaturated porous media.

164 The vapor flow continuity governing equation is given by

$$\frac{\partial}{\partial t}(\rho\theta_s) + \nabla \cdot \rho \left( - \frac{(1 - k_r)\kappa}{\mu} \nabla p \right) = 0 \quad (4)$$

165 Here  $\rho$  is the fluid density;  $\kappa$  is the saturated permeability of the soil matrix;  
 166  $\mu$  is the fluid viscosity; and  $p$  is the fluid pressure. We assume that the  
 167 contaminant vapors are so dilute that the gas flow properties can be taken  
 168 to be those of air, specifically at 20 °C. All the transport properties may be  
 169 found in Table 1.

*Boundary Conditions.* To solve (4) we assign the atmosphere boundary (see Figure 2) to be the reference pressure, i.e. zero pressure. The foundation crack boundary is assigned to be at the indoor-outdoor pressure difference value. Remaining boundaries are no-flow boundary conditions.

$$\text{Atmosphere} \quad p = 0 \text{ (Pa)} \quad (5)$$

$$\text{Foundation crack} \quad p = p_{\text{in}} - p_{\text{out}} = p_{\text{in}} \text{ (Pa)} \quad (6)$$

$$\text{All other} \quad -\vec{n} \cdot \rho \vec{u} = 0 \text{ (kg/(m}^2 \cdot \text{s))} \quad (7)$$

170 Here  $\vec{n}$  and  $\vec{u}$  are the boundary normal and gas velocity vectors.

171 *Initial Conditions.* For steady-state problems, the initial conditions do not  
 172 influence the solution. Transient simulations however, require initial condi-  
 173 tions and these are assumed to be given by the steady-state solution.

174 *2.2.3. Mass Transport In The Vadose Zone*

175 Contaminants in the vadose zone exist in three phases - gaseous, dissolved  
 176 in water, and sorbed onto soil particles. While there are three distinct phase  
 177 concentrations, the water and gas phases are related via Henry's Law (8).

$$c_g = K_H c_w \quad (8)$$

178 Where  $c_g$  and  $c_w$  are the gas and water phase concentrations respectively in  
 179 mol/m<sup>3</sup>;  $K_H$  is the dimensionless Henry's Law constant.

180 In this work, we consider sorption equilibrium between the soil and vapor  
 181 phases, to be governed by the water contaminant concentration (9).

$$c_s = K_{\text{ads}} \rho_b c_g = K_{\text{ads}} \frac{\rho}{1 - \theta_s} K_H c_w \quad (9)$$

182 Here the  $c_s$  is the solid phase concentration in mol/kg;  $\rho_b$  is the bulk density  
 183 of the soil kg/m<sup>3</sup>, which is given by the density  $\rho$  and the total soil porosity  
 184  $\theta_s$ ;  $K_{\text{ads}}$  is the vapor-solid sorption partition coefficient in m<sup>3</sup>/kg.

185 Mass transport in the vadose zone is governed by diffusion and advection  
 186 and is given by (10). It is important to note that this governing equation is  
 187 written in terms of the water phase contaminant concentration  $c_w$ , but via  
 188 Henry's Law and the vapor-solid sorption partition coefficient, it does in fact  
 189 describe the contaminant concentration and transport in all three phases.

$$R \frac{\partial c_w}{\partial t} = \nabla \cdot [D_{\text{eff}} \nabla c_w] - K_H \vec{u} \cdot \nabla c_w \quad (10)$$

190 The first term in (10) gives the change in contaminant water concentration  
 191 with respect to time, modified by the *retardation factor*,  $R$ , which is discussed  
 192 below; The second is the effective diffusive flux which is modified by the  
 193 effective diffusion coefficient  $D_{\text{eff}}$  which is also discussed below. The third is  
 194 the advective flux where  $\vec{u}$  is the soil-gas velocity from Darcy's Law, which  
 195 when multiplied with  $K_H$  gives the gas phase concentration advective flux,  
 196 e.g. advective transport only occurs in the vapor phase and not the liquid  
 197 phase (the water in the soil matrix is assumed to be at steady-state).

198 *Contaminant entry into the building.* The contaminant enters the building  
 199 through a combination of advection and diffusive fluxes and is given by (11).

$$j_{ck} = \begin{cases} u_{ck} c_g - \frac{D_{\text{air}}}{L_{\text{slab}}} (c_{in} - c_g) & u_{ck} \geq 0 \\ u_{ck} c_{in} - \frac{D_{\text{air}}}{L_{\text{slab}}} (c_{in} - c_g) & u_{ck} < 0 \end{cases} \quad (11)$$

200 Here the  $j_{ck}$  is the molar contaminant flux into the building in mol/(m<sup>2</sup> · s);  
 201  $D_{\text{air}}$  is the contaminant diffusion coefficient in pure air in m<sup>2</sup>/s;  $L_{\text{slab}}$  is the  
 202 thickness of the foundation slab in m. The flux expression changes if there  
 203 is a bulk flow into the building, i.e.  $u_{ck} \geq 0$ , or out of the building.



204 *Retardation factor.* As the contaminants are transported through the vadose  
 205 zone, the partitioning between the various phases increases the contaminant  
 206 residency time, retarding the transport of contaminants. This effect is rep-  
 207 resented by  $R$  which is the retardation factor (12).

$$R = \theta_w + \theta_g K_H + \rho_b K_H K_{\text{ads}} \quad (12)$$

208 Here  $\theta_w$ ,  $\theta_g$  are the water and gas filled soil porosities;  $K_{\text{ads}}$  is the vapor-solid  
 209 partition coefficient in  $\text{m}^3/\text{kg}$ .

210 *Effective diffusivity.* The effective diffusivity in the vadose zone varies with  
 211 the soil moisture content, from being close to that in water when fully sat-  
 212 urated and close to that in air when soil moisture is low. Millington-Quirk  
 213 developed (13) which describes the effective diffusivity in variably saturated  
 214 porous media.

$$D_{\text{eff}} = D_{\text{water}} \frac{\theta_w^{\frac{7}{3}}}{\theta_s^2} + \frac{D_{\text{air}} \theta_g^{\frac{7}{3}}}{K_H \theta_s^2} \quad (13)$$

215 Where the porosity terms reflect the water and gas phase tortuosity;  $D_{\text{air}}$  and  
 216  $D_{\text{water}}$  are the contaminant diffusion coefficient in air and water respectively  
 217 in  $\text{m}^2/\text{s}$ ; The Henry's Law constant  $K_H$  appears here to reflect that all the  
 218 contaminant transport is a function of the contaminant water concentration.

*Boundary Conditions.* In this model, the sole contaminant source is assumed  
 to be the homogenously contaminated groundwater, which we assume to have  
 a fixed concentration. The atmosphere acts as a contaminant sink and thus  
 this is simply a zero concentration boundary condition. Contaminants leave  
 the soil domain and enter the building through a combination of advective  
 and diffusive gas phase transport. The boundary condition applied to all  
 other boundaries is a no-flow boundary.

$$\text{Groundwater} \quad c_w = 0 \text{ (mol/m}^3\text{)} \quad (14)$$

$$\text{Atmosphere} \quad c_w = c_{gw} \text{ (mol/m}^3\text{)} \quad (15)$$

$$\text{Foundation crack} \quad -\vec{n} \cdot \vec{N} = -\frac{j_{ck}}{K_H} \text{ (mol/(m}^2 \cdot \text{s))} \quad (16)$$

$$\text{All other} \quad -\vec{n} \cdot \vec{N} = 0 \text{ (mol/(m}^2 \cdot \text{s))} \quad (17)$$

219  $\vec{n} \cdot \vec{N}$  is the dot product between the boundary normal vector and the contam-  
 220 inant flux;  $j_{ck}$  is the contaminant vapor flux into the building. We assume

221 that only contaminants in the gas phase enter the building, and dividing  $j_{ck}$   
 222 by  $K_H$  we get proper accounting in terms of the water phase concentration  
 223 accounting in the main transport equation 10.

224 *Initial Conditions.* For transient simulations in this work, the steady-state  
 225 solution to a corresponding case is always used as an initial condition.

#### 226 2.2.4. Indoor Environment

227 The indoor air space is modeled as a continuously stirred tank reactor  
 228 (CSTR) given by (29). Contaminants are assumed to only enter through  
 229 the foundation crack, represented by  $n_{ck}$ , which is calculated by integrating  
 230 the contaminant flux over the foundation crack boundary. The product of  
 231 air exchange rate, (which governs how many house volumes are exchanged  
 232 with the outside per time unit,) and indoor air contaminant concentration  
 233 gives the contaminant exit rate from the house. The sorption of contaminant  
 234 on indoor materials is given by the sorption term in (31) and the sorbed  
 235 contaminant concentration on all interior surfaces is given by (30).

$$V_{\text{bldg}} \frac{\partial c_{\text{in}}}{\partial t} = n_{\text{ck}} - A_e c_{\text{in}} V_{\text{bldg}} - r_{\text{sorb}} V_{\text{mat}} \quad (18)$$

$$V_{\text{mat}} \frac{\partial c_{\text{sorb}}}{\partial t} = r_{\text{sorb}} V_{\text{mat}} \quad (19)$$

$$r_{\text{sorb}} = k_1 c_{\text{in}} - k_2 c_{\text{sorb}} \quad (20)$$

$$n_{\text{ck}} = \int_{A_{ck}} j_{ck} dA \quad (21)$$

236 Here  $V_{\text{bldg}}$  and  $V_{\text{mat}}$  are the indoor control volume and volume of indoor  
 237 material in  $\text{m}^3$ ;  $c_{\text{in}}$  and  $c_{\text{sorb}}$  are the indoor and sorbed (onto the indoor ma-  
 238 terial) contaminant concentrations in  $\text{mol}/\text{m}^3$ ;  $n_{\text{ck}}$  is the contaminant entry  
 239 rate in  $\text{mol}/\text{s}$ , which is calculated by integrating the contaminant flux  $j_{ck}$   
 240 over the foundation crack area;  $r_{\text{sorb}}$  sorption rate in  $\text{mol}/(\text{m}^3 \cdot \text{s})$ ;  $k_1$  and  $k_2$   
 241 are the sorption and desorption rate constants in  $1/\text{s}$ .

242 *Fitting Kinetic Parameters.* These values of  $k_1$  and  $k_2$  are found by ap-  
 243 plying (31) numerically to the experimental data via least square fitting.  
 244 We use Runge-Kutta method of order 5(4) as the numerical solve, which  
 245 is implemented together with the least square method in the SciPy python  
 246 package[19].

Soil Properties[20, 21]						
Soil	$\kappa$ (m <sup>2</sup> )	$\theta_s$	$\theta_r$	$\alpha$ (1/m)	$n$	$\rho$ kg/m <sup>3</sup>
Sand	$9.9 \cdot 10^{-12}$	0.38	0.053	3.5	3.2	1460
Sandy Loam	$5.9 \cdot 10^{-13}$	0.39	0.039	2.7	1.4	1460
Trichloroethylene (diluted in air) Properties[20, 21]						
$D_{\text{air}}$ (m <sup>2</sup> /h)	$D_{\text{water}}$ (m <sup>2</sup> /h)	$\rho$ (kg/m <sup>3</sup> )	$\mu$ (Pa · s)	$K_H$		
$2.47 \cdot 10^{-2}$	$3.67 \cdot 10^{-6}$	1.614	$1.86 \cdot 10^{-5}$	0.403		
Building Properties						
$V_{\text{bldg}}$ (m <sup>3</sup> )	$L_{\text{slab}}$ (cm)	$A_e$ (1/hr)				
300	15	0.5				

Table 1: Transport and material properties used in the model. See Table 4 for nomenclature.

### 247 3. Results & Discussion

#### 248 3.1. Fitting Sorption Parameters

249 Figure 3 shows the result of fitting the sorption data for three select mate-  
250 rials - wood, Applying soil, and cinderblock concrete. The  $k_1$  and  $k_2$  represent  
251 the rates at which TCE sorbs and desorbs respectively onto/from the mate-  
252 rial of interest. The equilibrium partition constant, using the formulation in  
253 (31), is given by

$$K = \frac{k_1}{k_2} \quad (22)$$

254 and defines the sorption isotherm. Here a larger  $K$  indicates that there is a  
255 greater propensity for contaminant sorption.

256 To apply a soil sorption isotherm in (10)  $K$  needs to be converted to  
257 m<sup>3</sup>/kg. This is done by multiplying  $K$  isotherm with inverse of the soil bulk  
258 density  $\rho_b$ , which is taken to be 1460 kg/m<sup>3</sup>[21].

$$K_{\text{ads}} = \frac{K}{\rho_b} = 5.28 \text{ (m}^3/\text{kg)} \quad (23)$$

259 Table 2 shows the fitted parameters for the tested materials. Based on this  
260 these results we can see that cinderblock and soil have orders of magnitude  
261 larger sorption capacities than wood or drywall does. We can also see by that

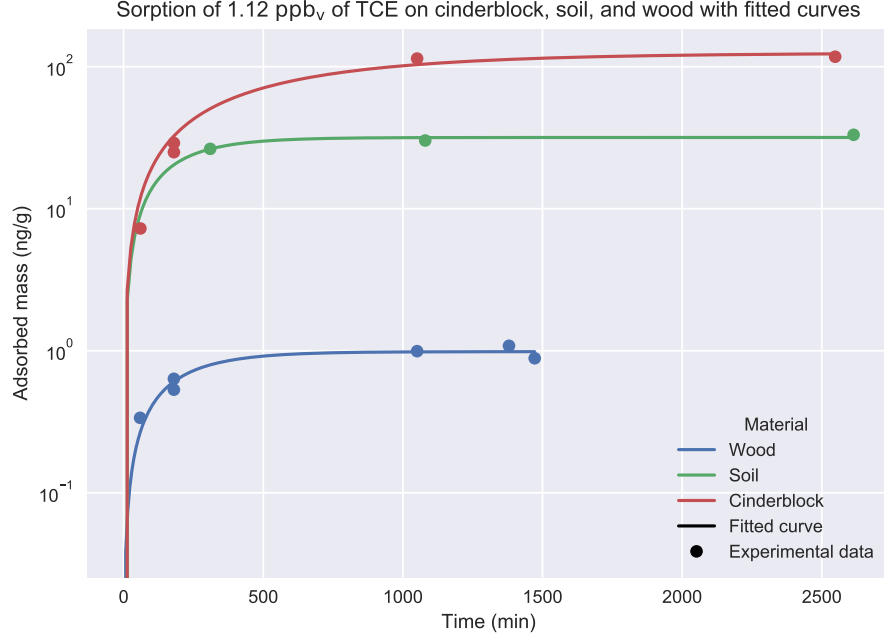


Figure 3: Experimental data of sorption of TCE onto three select materials as well as fitted sorption rates based on the kinetic model (31).

soil and cinderblock sorb quickly, much faster than a material with similar  
sorpative capacity such as paper.

Table 2: Fitted kinetic sorption parameters based on sorption experiment data. Six different types of materials are considered.  $k_1$  and  $k_2$  are the sorption and desorption constants respectively, and  $K$  is the sorption equilibrium constant.

Material	$k_1$ (1/hr)	$k_2$ (1/hr)	$K$
Wood	44.90	0.32	140.90
Drywall	87.94	0.41	214.87
Carpet	58.74	0.26	226.21
Paper	88.37	0.04	2195.69
Soil	2636.57	0.34	7702.94
Cinderblock	4175.16	0.10	41501.26

264 *3.2. Soil Sorption's Retarding Effect*

The effect of building pressurization is a key factor in VI that influences the advective contaminant transport into or out of the building. The magnitude of indoor contaminant concentration change in response to a pressurization change is significantly influenced by a variety of factors, such as soil permeability, foundation depth, soil moisture, and sorption. To investigate the effect that soil sorption has on contaminant soil mass transport in the VI context, we have run two types transient simulation where initially the modeled structure is depressurized at a steady -5 Pa to establish a steady-state baseline. At the start of the simulation, the building building is further depressurized to -15 Pa (24), or overpressurized to 15 Pa (25), and the simulation is allowed to run for 72 hours.

$$\text{Depressurization : } p_{\text{in}} = \begin{cases} -5, & t = 0 \text{ (hr)} \\ -15, & 0 < t \leq 72 \text{ (hr)} \end{cases} \quad (24)$$

$$\text{Overpressurization : } p_{\text{in}} = \begin{cases} -5, & t = 0 \text{ (hr)} \\ 15, & 0 < t \leq 72 \text{ (hr)} \end{cases} \quad (25)$$

265 For each of these cases, the simulation is run using two different soil types  
 266 - sand and sandy loam. Sand is assumed here to not sorb any TCE, while  
 267 for sandy loam a range of sorption isotherms are used. These range from  
 268 no sorption ( $K_{\text{ads}} = 0 \text{ (m}^3/\text{kg})$ ) to the experimentally determined sorption  
 269 isotherm for Applying soil ( $K_{\text{ads}} = 5.28 \text{ (m}^3/\text{kg})$ ). With the experimentally  
 270 determined isotherm, we see that the ratio between sorbed concentration and  
 271 soil-gas phase concentration is 7708, i.e. there is a much larger amount of  
 272 contaminant sorbed to the soil than present in the vapor phase of the vadose  
 273 zone. When  $K_{\text{ads}} = 5.28 \cdot 10^{-4} \text{ (m}^3/\text{kg})$  this ratio is roughly unity (0.77).

274 The top panel of Figure 4 shows the indoor air contaminant concentration  
 275 as the simulated building is undergoing the depressurization as represented  
 276 by the equation (24) case. results are plotted as attenuation of contaminant  
 277 relative to the groundwater source, i.e.

$$\alpha_{\text{gw}} = \frac{c_{\text{in}}}{c_{\text{gw}} K_H} \quad (26)$$

278 Here we can see that when the surrounding soil consists of sand, the indoor  
 279 concentration increases rapidly as the building is depressurized. The increase  
 280 is significantly smaller for the sandy loam cases, and becomes smaller as the  
 281 sorbed mass increases ( $K_{\text{ads}}$  increases).

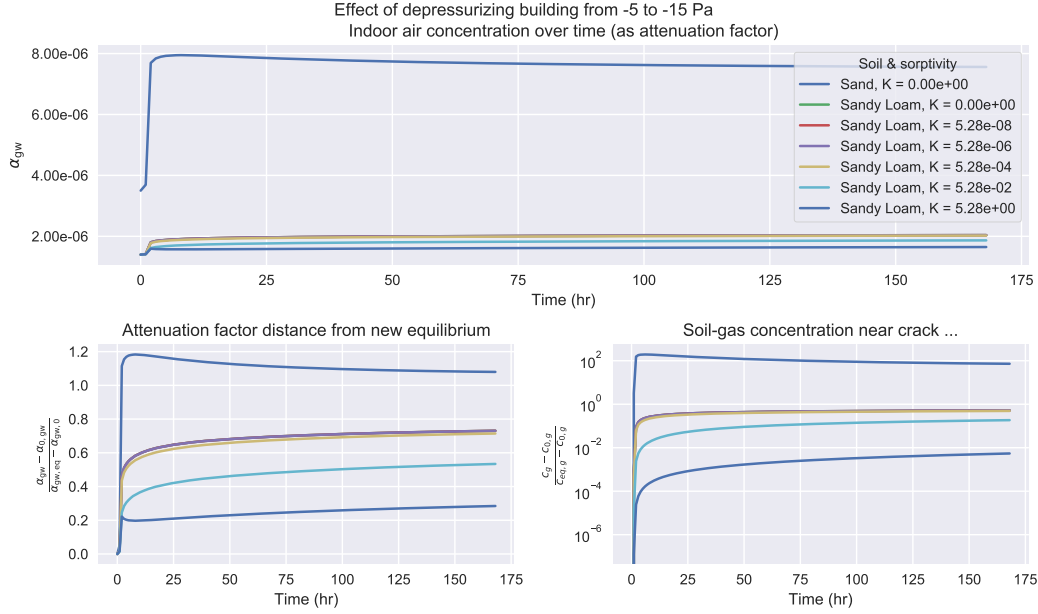


Figure 4

282 The bottom left panel shows the time for reaching the new equilibrium.  
 283 At the start of the simulation, the building starts at an attenuation of  $\alpha_{gw,0}$ ,  
 284 which is the steady-state concentration when the building is depressurized to  
 285 -5 Pa. As the building is further depressurized to -15 Pa, the indoor air con-  
 286 centration will approach a new equilibrium state  $\alpha_{gw,eq}$  (the result of which is  
 287 obtained from a steady-state simulation at that depressurization). By plot-  
 288 ting  $\frac{|\alpha_{gw} - \alpha_{gw,0}|}{|\alpha_{gw,eq} - \alpha_{gw,0}|}$  we can see how far away we are from the new equilibrium  
 289 state, and a value of 0 represents that we are at the initial concentration,  
 290 i.e.  $\alpha_{gw} = \alpha_{gw,0}$ , and a value of 1 represents  $\alpha_{gw} = \alpha_{gw,eq}$ , i.e. that the new  
 291 equilibrium has been reached. This demonstrates that times of hundreds of  
 292 hours may be needed to attain a near steady-state

293 The results of the same calculations are shown in the bottom right panel  
 294 as well, but instead of plotting the indoor air concentration, we consider the  
 295 average soil-gas concentration in a 5 cm diameter cylinder that envelops the  
 296 entire perimeter crack. The choice of 5 cm is arbitrary, but helps illustrate  
 297 what happens in the near-foundation-crack region. Examining these changes  
 298 allow us to better understand how the contaminant is transported into the  
 299 building from the soil. Consistent with the long timescales for the indoor air

300 to "adjust" to a new condition, the soil which is a significant source/sink for  
 301 the contaminant share a similar slow adjustment.

302 Before discussing the role of sorption, we can first compare the non-  
 303 sorbing sand and sandy loam cases. Due to its higher permeability and  
 304 lower moisture content, sand is significantly more permeable to gas flow than  
 305 sandy loam (see Table 1 for permeability values). Consequently the advective  
 306 transport through the foundation crack is much more significant in the sand  
 307 case than the sandy loam case. This may be characterized by a Péclet number  
 308 for transport through the foundation crack, where

$$\text{Pe} = \frac{\text{advection}}{\text{diffusion}} = \frac{u_{\text{ck}} L_{\text{slab}}}{D_{\text{air}}} \quad (27)$$

309 and the Péclet number is around 4 versus 0.2 at a -15 Pa depressurization for  
 310 sand and sandy loam respectively. A Péclet greater than one indicate that  
 311 advective transport dominates and vice versa.

312 Due to the advection dominated transport mechanism in the sand case,  
 313 the indoor air concentrations are temporarily elevated above the final equi-  
 314 librium concentration at -15 Pa. (Note that the absolute distance from equi-  
 315 librium is plotted in Figure 4 which is why the concentration is two order of  
 316 magnitude dispalced.) This phenomena occurs because initially more con-  
 317 taminants are drawn into the building from the near crack area than can be  
 318 resupplied, temporarily depleting the local soil-gas contaminant concentra-  
 319 tion.

320 One can notice that many of the sandy loam lines overlap, and start  
 321 diverging from each other when  $K_{\text{ads}} = 5.28 \cdot 10^{-4}$  ( $\text{m}^3/\text{kg}$ ), at the point  
 322 where the ratio of sorbed and soil-gas concentration are roughly equal. Since  
 323 the indoor air concentration depend on the soil-gas concentration, this is the  
 324 origin of the difference.

325 The reason for this is that it is at this threshold the that sorptive contri-  
 326 bution to the retardation factor (12) starts to becomes larger than the other  
 327 terms.

$$\rho_b K_H K_{\text{ads}} > \theta_w + \theta_g K_H \quad (28)$$

328 Thus it is at this point that the contaminant transport, i.e. replenishment  
 329 from the source in the soil starts to become retarded by sorption. The parti-  
 330 tioning between the various phases controls residence time as the contaminant  
 331 is transported. Under VI conditions, the values of  $\theta_w + \theta_g K_H$  are relatively  
 332 small values, while  $K_{\text{ads}}$  can vary by orders of magnitude, making sorption  
 333 potentially a very significant retarder for soil transport.

334 We can also note that the retarding effect of sorption also somewhat  
 335 depends on the contaminants Henry's Law constant  $K_H$ , bulk density  $\rho_b$   
 336 and the moisture content  $\theta_w$ . For instance if the local temperature is higher,  
 337 then contaminant  $K_H$  is likewise larger, and the retardation factor is greater.  
 338 Generalizing this is difficult however, as  $K_{ads}$  decreases with temperature,  
 339 and the interplay between these may be complicated. Nevertheless this hints  
 340 that there may be a climate/weather component to how significantly sorption  
 341 induced retardation is.

342 Figure 5 shows the same sort of analysis as in Figure 4 but with the  
 343 building pressurization as described by (25). As the building is overpres-  
 344 surized, the indoor contaminant is pushed back out into the soil. Since the  
 345 indoor air concentration is lower than the soil-gas concentration, a drop in  
 346 local soil-gas concentration is observed along with a decrease in indoor air  
 347 contaminant concentration.

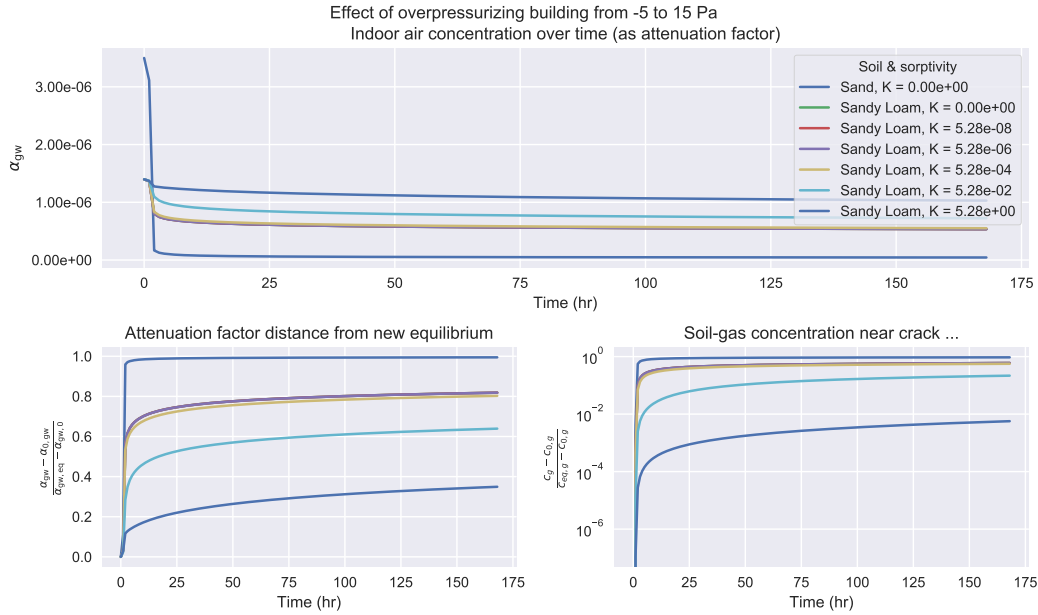


Figure 5

### 348 3.3. Effects of Indoor Material Sorption

349 For these simulations we assume that there is no soil sorption. We con-  
 350 sider the basement (the indoor air space) and assume that the inside surfaces



are entirely made up of one of the materials we presented in 3.1. We also assume that the material covering the indoor surfaces has a certain thickness or depth that the contaminants can penetrate - providing a certain volume or mass of sorbing material in the indoor environment. Table 3 shows the surface area, penetration depth, and volume of each material studied. While the assumptions regarding coverage of different portions of the space are arbitrary, they are of the right order of magnitude and they do present some limiting cases of the potential effect of sorption onto/from these materials.

Material	$d_p$ (mm)	$V_{\text{mat}}$ (m <sup>3</sup> )
Cinderblock	5	1.6
Wood	1	0.32
Drywall	10	3.2
Carpet	10	3.2
Paper	0.1	0.032

Table 3: The assumed contaminant penetration depth and subsequent volume of the sorbing indoor materials. The material surface area is assumed to be the same, and each material completely cover the surfaces of a 10x10x3 meter room.

The modeled building then undergoes a pressurization cycle, in which at start of the simulation it has been depressurized at -5 Pa at steady-state. The building is then sequentially depressurized to -15 Pa, then pressurized to 15 Pa, and finally again depressurized to -5 Pa. For each sequence, the new pressurization is maintained for 24 hours. This pressurization cycle may be seen in the top left panel of 6. The choice of pressurization cycle is somewhat arbitrary, but can be used to represent limiting cases of natural pressurization variation, or artificially induced pressurization. Figure 6 shows the result of these simulations.

The change in indoor air contaminant concentration over this pressurization cycle is shown in the bottom panel of Figure 6. First we consider the reference case - where there is no sorbing indoor materials present. (The blue line is the reference case, which may be difficult to see as the wood and carpet lines overlap.) Here we see that as the building is depressurized, the indoor air contaminant concentration increases quickly in response to the depressurization change, and is approaching a new equilibrium.

The presence of the various studied building materials in the indoor environment have very different effects on the change in indoor air contaminant

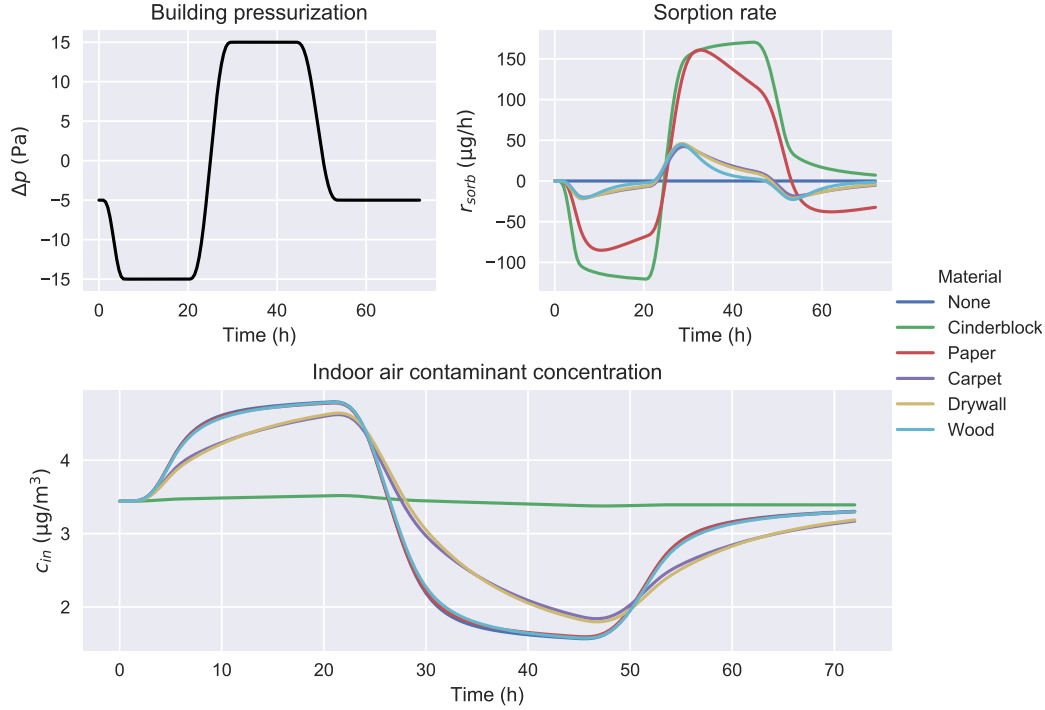


Figure 6: Comparison of how sorption onto/from various indoor materials affect the indoor air contaminant concentration (bottom) of a building that undergoes a pressurization cycle (top left). The rate of de- and sorption for each considered material during the cycle are also shown (top right) and is governed by (31). A positive value means that contaminant vapors are being sorbed onto/into the material and a negative means the material is desorbing into the indoor air space.

377 concentration. The presence of wood and carpet has little effect on the  
 378 indoor air concentration, whereas cinderblock has a very significant effect,  
 379 dampening out almost any change in indoor concentration. Drywall and car-  
 380 pet significantly delay the rate of change in the indoor concentration, but for  
 381 each 24 hour cycle, roughly the same indoor concentration is reached as in  
 382 the no sorbing material reference case.

383 The disparity in these result is explained by the the top right panel of  
 384 Figure 6. Here the de- and sorption rates in  $\mu\text{g}/\text{hr}$  for each indoor material  
 385 is shown. A positive and negative value here indicate that contaminant is  
 386 desorbed from or sorbed to the material respectively. To understand this  
 387 figure, it is useful to refer back to Table 2 which shows the sorption and  
 388 desorption rate constant  $k_1$  and  $k_2$  respectively, and the sorption equilibrium

389 constant  $K$  (a larger value indicate a larger sorptive capacity).

390 First we consider to the depressurization part of the cycle (1-25 hours).  
391 As in the indoor concentration panel, we see that the wood, drywall, and car-  
392 pet cases overlap. These materials have similar sorptive capacities ( $K$ ) and  
393 sorptive rates ( $k_2$ ). Paper, by contrast, has a similar shape to the previous  
394 three but its magnitude is significantly larger. This is because the  $K$  value  
395 for paper is one order of magnitude larger, indicating that wood, drywall, and  
396 carpet saturate with contaminant vapors over the time period, while paper  
397 does not. Cinderblock has a further order of magnitude larger  $K$  value, thus  
398 is even further away from being saturated, which is consistent with its even  
399 faster sorption rate.

400 Next we consider the overpressurization period (25-49 hours). Again we  
401 see here that wood, drywall, and carpet behave the similarly. This means  
402 that these reach the new contaminant saturation equilibrium at roughly the  
403 same time.

404 Here it is important to note that due to diffusion dominated transport  
405 through the foundation crack, even though the building is overpressurized,  
406 there is still substantial contaminant entry. And because the sole contam-  
407 inant source is contaminated groundwater, the sorbed equilibrium is deter-  
408 mined by this entry rate.

409 Paper and cinderblock initially behave very similarly during the overpres-  
410 surization period and desorb contaminants quickly. However, paper reaches  
411 its saturation limit after a relatively short time, while cinderblock has not  
412 even at the end of the overpressurization cycle. Since the desorption rate con-  
413 stants  $k_2$  are relatively similar for the materials, this disparity is primarily  
414 due to the different sorption equilibrium constants  $K$ .

415 Lastly, we consider the final period where the pressurization goes back  
416 to its initial state (49-72 hrs). Here we see that the reference case does not  
417 quite return to the initial indoor concentration. Thus the contaminant entry  
418 rate has not equilibrated yet, because the soil contaminant concentration has  
419 not done so either. As in the previous analysis we again see that the wood,  
420 drywall, and carpet cases don't differ from the reference. Paper is slightly  
421 different, for the same reasons that have already been discussed. Cinderblock  
422 is unique here, as it is releasing contaminants, due to the previous change  
423 in contaminant concentration. In other words, it is acting as a significant  
424 capacitance in the system.

425 From this simulation work the varied the effects of sorbing indoor mate-  
426 rials are apparent. Most of the tested materials only have a moderate effect

on the indoor air contaminant concentration dynamics, with the notable exception of cinderblock, which effectively maintains as pseudo-steady-state. However we also see from the analysis of the sorption dynamics that the desorption and sorption rate constants  $k_1$  and  $k_2$  are less important than the overall sorptive capacity  $K$  of the material.

### 3.4. Indoor Material Sorption And Mitigation

The work done by us and others has shown the large sorptive capacities of various common materials. The desorption of the sorbed contaminants may have significant impact on the apparent efficacy of various mitigation systems. To investigate this we consider a scenario where initially the modeled building is depressurized at -5 Pa and at the start of the simulation some perfect mitigation scheme is implemented and the contaminant entry  $n_{\text{entry}}$  in (29) goes to zero. We also assume that for each case, the indoor environment contains the same amount of indoor material as described in section 3.3. The air exchange rate is assumed to remain a constant 0.5 per hour for the entire simulation time.

Hence, we can drop  $n_{\text{ck}}$  in (29) and the equations used to model the indoor concentration becomes:

$$V_{\text{bldg}} \frac{\partial c_{\text{in}}}{\partial t} = A_e c_{\text{in}} V_{\text{bldg}} - r_{\text{sorb}} V_{\text{mat}} \quad (29)$$

$$V_{\text{mat}} \frac{\partial c_{\text{sorb}}}{\partial t} = r_{\text{sorb}} V_{\text{mat}} \quad (30)$$

$$r_{\text{sorb}} = k_1 c_{\text{in}} - k_2 c_{\text{sorb}} \quad (31)$$

This system of ordinary differential equations can be solved analytically. A solution to this is

$$\begin{bmatrix} c_{\text{in}} \\ c_{\text{sorb}} \end{bmatrix} = A \exp(\lambda_1 t) \vec{v}_1 + B \exp(\lambda_2 t) \vec{v}_2 \quad (32)$$

and finding the eigenvalues ( $\lambda_1, \lambda_2$ ) and eigenvectors ( $\vec{v}_1, \vec{v}_2$ ) of the system above, allows us to calculate the indoor and sorbed contaminants concentrations through time.  $A$  and  $B$  are constants found using the initial conditions

$$c_{\text{in}}(t = 0) = c_{\text{in},0} \rightarrow A \quad (33)$$

$$c_{\text{sorb}}(t = 0) = c_{\text{sorb},0} K \rightarrow B \quad (34)$$

where we assume that  $c_{\text{in},0} = 2 \text{ } (\mu\text{g}/\text{m}^3)$ .

446 The decrease in indoor air concentration (as attenuation factor  $\alpha_{gw}$ ) for  
 447 each case is seen in the top panel of Figure 7. As expected, when there is  
 448 no sorbing indoor materials, i.e. our reference case, the indoor concentration  
 449 decreases log-linearly. We can also see that contaminant desorption from  
 450 materials maintains a higher indoor air concentration relative to reference,  
 451 with cinderblock again shown to have the great impact.

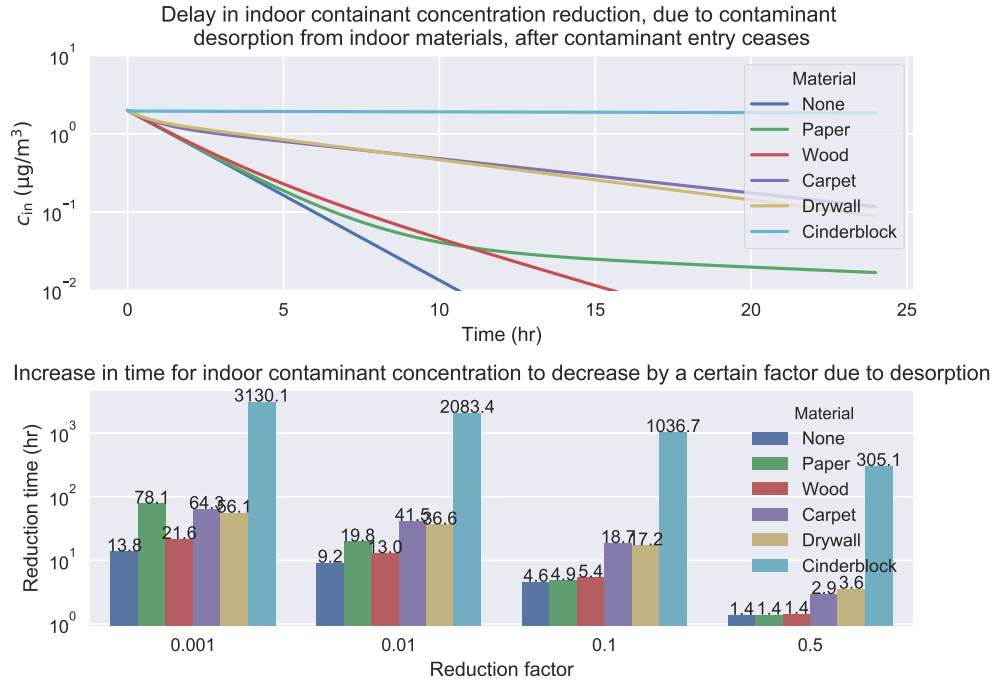


Figure 7: Contaminant desorption from indoor materials delay the decrease in indoor contaminant concentration after a mitigation system has been implemented. The top panel shows the indoor air concentration after system implementation, considering desorption from different materials. The bottom panel quantifies how long it takes for the indoor concentration to decrease by a certain factor, considering the different cases.

452 Clearly, the contaminant desorption from indoor materials can signifi-  
 453 cantly delay the time that a certain reduction in indoor air concentration  
 454 after a successful mitigation system has been implemented. In the bottom  
 455 panel of Figure 7 we quantified the number of hours for a fifty percent, a  
 456 one, and two orders of magnitude reduction in indoor air concentration to  
 457 occurs, both absent sorbing indoor materials (the reference case) and in the  
 458 presence of the one's presented earlier in this work. On the x-axis the indoor

459 air concentration reduction factor is shown, and on the y-axis the number of  
460 hours for the specified reduction occur is displayed, for each material. The  
461 number of hours for each case are also shown at the top of each bar.

462 From this, we see that it takes 1.4 hours for the a 50% reduction in indoor  
463 air concentration to occur for the reference, paper, and wood cases, while this  
464 time increases up to 305 hours in the cinderblock case. This indicates the  
465 significant effect that sorption of TCE onto cinderblock can potentially have  
466 on the efficacy on a VI mitigation scheme, with the remaining materials  
467 having a relatively minor or moderate effect; a trend we have seen in other  
468 parts of this work.

#### 469 4. Conclusions

470 The work presented here offers new insights into how sorption effect may  
471 influence VI; exploring how sorption affects VI fundamentally and in some  
472 applications. Based on what has been presented here, we can draw some  
473 conclusions.

- 474 • The sorption and desorption kinetics, while they vary quite a bit, do not  
475 seem to make a significant difference in most VI applications or cases,  
476 at least not the ones considered here. But, what has been apparent is  
477 that it is the sorption capacities of the particular material that matters,  
478 although these seem to have to be on the same scale as cinderblock to  
479 truly be significant.
- 480 • The sorptive capacities of materials vary significantly and it may not  
481 be obvious which ones have large sorptive capacities and which do not.  
482 More materials, in combination with other contaminants, need to be  
483 tested to gain a more comprehensive understanding of which materials  
484 are of particular concern in VI.
- 485 • Sorption fundamentally retards contaminant transport in soils, effec-  
486 tively increasing the residence time of the contaminant in the soil. How-  
487 ever, sorption will only start to retard transport if the sorption partition  
488 coefficient is large enough to exceed the "naturally" induced residence  
489 by the soil moisture content. Sorption on materials in the indoor en-  
490 vironment functions in a similar way, and like a capacitance, inhibits  
491 changes in indoor concentration. These particular phenomena may be  
492 relevant to consider if one wants to try to influence the contaminant

493 transport and entry rate into the building via forceful pressurization  
494 of the building, e.g. the controlled pressure method, as these attempts  
495 may be less effective than expected due to sorption.

- 496 • Contaminant desorption from indoor materials may also have a signifi-  
497 cant effect of mitigation systems, potentially delaying effective mitiga-  
498 tion from taking place from a matter of hours to several days or weeks,  
499 depending on the amount and kind of indoor materials present.

## 500 **Acknowledgements**

501 This project was supported by grant ES-201502 from the Strategic Envi-  
502 ronmental Research and Development Program and Environmental Security  
503 Technology Certification Program (SERDP-ESTCP).

504 Declaration of interest: none

## 505 References

- 506 [1] R. Meininghaus, L. Gunnarsen, H. N. Knudsen, Diffusion and Sorp-  
507 tion of Volatile Organic Compounds in Building Materials-Impact on  
508 Indoor Air Quality, *Environ. Sci. Technol.* 34 (15) (2000) 3101–3108.  
509 doi:10.1021/es991291i.
- 510 [2] R. Meininghaus, E. Uhde, Diffusion studies of VOC mixtures in a build-  
511 ing material, *Indoor Air* 12 (4) (2002) 215–222. doi:10.1034/j.1600-  
512 0668.2002.01131.x.
- 513 [3] F. D. Tillman, J. W. Weaver, Review of Recent Research on Vapor  
514 Intrusion (2005) 47.
- 515 [4] X. Wang, Y. Zhang, J. Xiong, Correlation between the solid/air  
516 partition coefficient and liquid molar volume for VOCs in build-  
517 ing materials, *Atmospheric Environment* 42 (33) (2008) 7768–7774.  
518 doi:10.1016/j.atmosenv.2008.05.030.
- 519 [5] J. Xu, J. S. Zhang, X. Liu, Z. Gao, Determination of partition and  
520 diffusion coefficients of formaldehyde in selected building materials and  
521 impact of relative humidity, *J. Air Waste Manag. Assoc.* 62 (6) (2012)  
522 671–679. doi:10.1080/10962247.2012.665812.
- 523 [6] A. Bodalal, J. S. Zhang, E. G. Plett, A method for measuring internal  
524 diffusion and equilibrium partition coefficients of volatile organic com-  
525 pounds for building materials, *Building and Environment* 35 (2) (2000)  
526 101–110. doi:10.1016/S0360-1323(99)00005-0.
- 527 [7] U.S. Environmental Protection Agency, OSWER Technical Guide for  
528 Assessing and Mitigating the Vapor Intrusion Pathway From Subsurface  
529 Vapor Sources To Indoor Air (2015).
- 530 [8] C. Holton, Y. Guo, H. Luo, P. Dahlen, K. Gorder, E. Dettenmaier,  
531 P. C. Johnson, Long-Term Evaluation of the Controlled Pressure Method  
532 for Assessment of the Vapor Intrusion Pathway, *Environ. Sci. Technol.*  
533 49 (4) (2015) 2091–2098. doi:10/f64j45.
- 534 [9] C. C. Lutes, R. S. Truesdale, B. W. Cosky, J. H. Zimmerman,  
535 B. A. Schumacher, Comparing Vapor Intrusion Mitigation System



- 536 Performance for VOCs and Radon, *Remediation* 25 (4) (2015) 7–26.  
537 doi:10/gd6dfn.
- 538 [10] U.S. Environmental Protection Agency, Assessment of Mitigation Sys-  
539 tems on Vapor Intrusion: Temporal Trends, Attenuation Factors, and  
540 Contaminant Migration Routes under Mitigated And Non-mitigated  
541 Conditions (2015).
- 542 [11] T. McHugh, P. Loll, B. Eklund, Recent advances in vapor intrusion  
543 site investigations, *Journal of Environmental Management* 204 (2017)  
544 783–792. doi:10/gd6dgk.
- 545 [12] P. C. Johnson, R. A. Ettinger, Heuristic model for predicting the intru-  
546 sion rate of contaminant vapors into buildings, *Environ. Sci. Technol.*  
547 25 (8) (1991) 1445–1452. doi:10/d9cbhd.
- 548 [13] J. C. Little, J. M. Daisey, W. W. Nazaroff, Transport of subsurface  
549 contaminants into buildings, *Environ. Sci. Technol.* 26 (11) (1992) 2058–  
550 2066. doi:10/dfg5dc.
- 551 [14] E. Shirazi, K. G. Pennell, Three-dimensional vapor intrusion modeling  
552 approach that combines wind and stack effects on indoor, atmospheric,  
553 and subsurface domains, *Environ. Sci.: Processes Impacts* 19 (12) (2017)  
554 1594–1607. doi:10/gd6df3.
- 555 [15] R. Shen, K. G. Pennell, E. M. Suuberg, A numerical investigation of  
556 vapor intrusion — The dynamic response of contaminant vapors to  
557 rainfall events, *Science of The Total Environment* 437 (2012) 110–120.  
558 doi:10/f4fp9s.
- 559 [16] J. G. V. Ström, Y. Guo, Y. Yao, E. M. Suuberg, Factors affect-  
560 ing temporal variations in vapor intrusion-induced indoor air contam-  
561 inant concentrations, *Building and Environment* 161 (2019) 106196.  
562 doi:10.1016/j.buildenv.2019.106196.
- 563 [17] M. T. van Genuchten, A Closed-form Equation for Predicting the Hy-  
564 draulic Conductivity of Unsaturated Soils, *Soil Sci. Soc. Am.* 44 (5)  
565 (1980) 892–898. doi:10/fdc8mc.
- 566 [18] C. W. Fetter, *Contaminant Hydrogeology*, Macmillan Publishing Com-  
567 pany, 1993.

- 568 [19] E. Jones, T. Oliphant, Pearu Peterson, SciPy: Open source scientific  
569 tools for Python (2011).
- 570 [20] L. D. V. Abreu, H. Schuver, Conceptual Model Scenarios for the Vapor  
571 Intrusion Pathway (2012).
- 572 [21] U.S. Environmental Protection Agency, Users's Guide For Evaluating  
573 Subsurface Vapor Intrusion Into Buildings (2004).

---

$A_{\text{ck}}$	Crack area
$A_e$	Air exchange rate
$\alpha, n, m, l$	van Genuchten parameters
$\alpha_{\text{gw}}$	Attenuation from groundwater contaminant vapor source
$c_{\text{in}}$	Indoor air contaminant concentration
$c_w$	Soil-water contaminant concentration
$c_g$	Soil-gas contaminant concentration
$c_s$	Sorbed contaminant concentration in the soil
$c_{\text{sorb}}$	Sorbed contaminant concentration on indoor material
$c_{\text{gw}}$	Contaminant groundwater concentration
$D_{\text{eff}}$	Effective diffusion coefficient
$D_{\text{air}}, D_{\text{water}}$	Diffusion coefficient in air/water
$d_p$	Penetration depth of sorbed contaminant in material
$j_{\text{ck}}$	Contaminant molar flux through the foundation crack
$\kappa$	Saturated soil permeability
$K_{\text{ads}}$	Sorption partition coefficient in soil
$K$	Sorption partition coefficient
$K_H$	Dimensionless Henry's law constant
$k_r$	Relative permeability
$L_{\text{slab}}$	Thickness of the foundation slab
$\lambda$	Eigenvalue
$M$	Molar mass
$\mu$	Contaminant vapor viscosity
$n_{\text{ck}}$	Contaminant entry rate through the foundation crack
ppb <sub>v</sub>	Part-per-billion by volume
$p$	Pressure in soil
$p_{\text{in}}$	Indoor pressure relative to outside
$p_{\text{out}}$	Ambient outside pressure
$\rho$	Density
$\rho_b$	Bulk density
$R$	Retardation factor
$r_{\text{sorb}}$	Rate of sorption
Se	Soil water saturation
$\theta_g$	Vapor/gas filled porosity
$\theta_w$	Water filled porosity
$\theta_r$	Residual water filled porosity
$\theta_s$	Saturated or total porosity
$\vec{u}$	Soil-gas velocity (vector quantity)
$u_{\text{ck}}$	Soil-gas velocity through the foundation crack
$V_{\text{bldg}}$	Building/control volume
$V_{\text{mat}}$	Volume of sorbing material
$\vec{v}$	Eigenvector
$z$	Elevation above groundwater

---

Table 4: List of abbreviations and nomenclature